Environmental Science and Pollution Research (2022) 29:71136–71149
https://doi.org/10.1007/s11356-022-20470-0

RESEARCH ARTICLE

Modeling impacts of mining activity-induced landscape change on local climate

Hongru Bi[1] · Wei Chen[1] · Jun Li[1] · Junting Guo[2] · Changchao She[3]

Received: 9 December 2021 / Accepted: 22 April 2022 / Published online: 20 May 2022

Abstract

As a major energy source, coal has been mined on an increasingly larger scale as the social economy has continuously developed, resulting in drastic land type changes. These changes in turn cause changes in the local climate and affect the local ecological environment. Therefore, for coal cities, mining activities are an important factor influencing the local climate, and clarifying the impact of mining activities on the ecological environment is important for guiding regional development. In this paper, the impact of land use/cover changes (LUCCs) on local temperature in the spring and summer seasons from 1980 to 2018 was simulated using the Weather Research and Forecasting (WRF) model with Xilinhot city as the study area, and the regional distribution of local surface energy was analyzed in conjunction with the ground-air energy transfer process. The results show that the grassland area in Xilinhot remained above 85% from 1980 to 2018, so mining activities had a small impact on the average temperature of the whole region. However, in the mining area, the warming effect caused by mining activities was more obvious, with an average temperature increase of 0.822 K. Among other land transformation types, the conversion to water bodies had a very obvious cooling effect, lowering the temperature by an average of 2.405 K. By comparing the latent heat flux (LH), sensible heat flux (SH), and ground heat flux (GRD) under different land use types, it was found that in 2018, the LH decreased by 0.487 W/m^2, the SH decreased by 0.616 W/m^2, and the GRD decreased by 0.753 W/m^2. The conversion to built-up urban land caused a significant decrease in the LH in the corresponding area, allowing more energy to be used to increase SH values, which resulted in significantly higher urban temperatures than in other areas.

Keywords Xilinhot · WRF · LUCC · Average temperature · Ground gas energy transfer

Introduction

Coal resources are currently the most abundant and widely distributed conventional energy source in the world. In recent years, rapid economic development and a significant increase in the human demand for energy have triggered a significant expansion of surface mining worldwide (Inta et al. 2020; Li et al. 2015; Qian et al. 2018; Schueler et al. 2011), and surface mining has shown continuous growth worldwide, especially in India and China (Larondelle and Haase 2012). This growth has been accompanied by serious damage to surface properties from coal mining, which have produced a series of environmental problems, such as surface collapse, soil erosion, and vegetation destruction (Wang et al. 2014). Scholars have conducted some research to address the surface ecological changes in mining areas; for example, Wu et al. used Shandong as the study area, obtained data on coal mining subsidence areas by image algorithms, and analyzed the impact of changes before and after coal mine surface collapse on surface landscape changes (Wu et al. 2009). Wu Qunying et al. used the ecologically fragile mining area in Shaanxi as the study area, used a combination of on-site actual soil moisture measurements and statistical analysis, and found that the changes in the surface soil water content above the mining area were basically consistent with the dynamic development pattern of dynamic ground fractures on the

Responsible Editor: Philippe Garrigues

✉ Jun Li
junli@cumtb.edu.cn

[1] College of Geoscience and Surveying Engineering, China University of Mining & Technology, Beijing 100083, China

[2] State Key Laboratory of Water Resource Protection and Utilization in Coal Mining, Beijing 102209, China

[3] Shenhua Beidian Shengli Energy Co., Ltd., Xilinhot 026000, China

surface (Wu et al. 2020). Tingting Wei et al. analyzed the physical properties and soil crusting within 1 year and 3 years after coal mining at the oversized working face in the Mu Us wind and sand area through sample site investigation and indoor analysis and found that the physical properties at the open-cut point received a stronger influence from mining than the mining face (Wei et al. 2015). Wei Jiansheng et al. investigated whether surface collapse caused by coal mining affects soil moisture properties, and the results showed that in coal mining areas, surface collapses in precipitation areas are significantly fewer than those in non-collapse areas (Wei et al. 2006). Zhang Yanxu et al. studied the soil moisture distribution characteristics of coal mining fracture areas by the methods of fixed-point location tracking and detection of fractures and found that coal mining subsidence fractures caused a decrease in soil moisture content, and the soil moisture content in both ground fracture and fracture-free areas within the subsidence area was less than that in unmined areas (Zhang et al. 2015). Xiang et al. quantified the change in the surface mining area based on the Chinese cover database and found that the rapid expansion of surface mining resulted in a significant decrease in natural habitat area, water retention capacity, net primary productivity, and food production (Xiang et al. 2021).

The above studies have shown that coal mining affects not only the surface conditions but also the local climate by changing the land cover type, and some scholars have conducted detailed and in-depth studies on the environmental impacts of land cover type changes (Bollasina and Nigam 2011; Xiu et al. 2018). Pielke and Brovkin found that land use types mainly affect the climate system by emitting or absorbing greenhouse gases into the atmosphere and changing the carbon cycle process (Alam et al. 2020). Notaro, Findell, and Wang found that land use/cover changes (LUCCs) can affect the climate by altering the precipitation distributed among evapotranspiration, runoff, and soil water during land surface processes (Wang et al. 2017). Biogeochemical processes, such as albedo and evapotranspiration, at the surface and biogeochemical processes, such as carbon cycling and greenhouse gas emissions, affect the climate at local, regional, and global scales and at different spatial and temporal scales (Liu et al. 2011).

Studies focusing on the impact of LUCCs on climate change can be divided into two main types: observational studies and simulation studies. For observational studies, it is difficult to separate information on the impact of LUCCs on the local climate from the general context of global changes, and we cannot accurately analyze the local impact of local LUCC changes. The main problem of simulation studies is the uncertainty of parameters in physical processes. Currently, most of the simulation work has used ideal sensitive land cover experiments, such as that of Wang, who based their research on weather research and forecasting (WRF) simulations of the climatic effects of LUCCs from 2001 to 2008 and concluded that LUCCs increased the temperature in most regions of China (Ma et al. 2009); Wang Mingna et al. used WRF simulations to analyze the effects of LUCCs on surface temperature in the semiarid region of northern China from 2001 to 2010, and concluded that LUCCs led to a decrease in local multiyear average temperature (Wang et al. 2016). Ying Zheng et al. simulated the effect of vegetation reconstruction on the regional climate in the Maowusu Desert region by incorporating high-resolution remotely sensed vegetation data into a WRF model and found that the average decrease in near-surface temperature ranged from 0.12 to 0.32°C (Zheng et al. 2020).

Xilinhot is located in the central part of the Inner Mongolia Plateau, and in recent years, with coal mining activities, the local land cover types have changed significantly, and environmental pollution and ecological degradation have become increasingly serious. The spatial resolution of land cover type data used in previous studies on this area is low, which is not satisfactory for studying the influence of subsurface type changes on surface temperatures in small- and medium-scale areas, and as a result, a more continuous study of spatial and temporal changes in temperature is lacking. The main objectives of this paper are (1) to utilize land use data with a spatial resolution of 30 m as the input data of the model subsurface to improve the simulation accuracy of the model for the local environment; (2) to discuss the degree of influence of different subsurface types on temperature; and (3) to explain the causal mechanism of subsurface types on temperature from the perspective of energy balance to provide scientific and reasonable opinions to support a deeper study on the influence of surface changes on the climate in mining areas in the future.

Data and methodology

Study area

Xilinhot city is located in the middle of the Xilinguol grassland in Inner Mongolia at a latitude of 43° 02′~44° 52′ north and a longitude of 115° 13′~117° 06′ east, has a medium-temperate semiarid continental climate, and is the political, economic, and cultural center of the Xilingol League. The city has a total area of 14,785 km^2, a total existing population of 177,000, and a gross regional product of 5.088 billion yuan (Chen and Liu 2006; Pang and Shun 2011; Pang and Su 2010). The region contains China's first nature reserve, Xilinguol Nature Reserve (Fig. 1). Moreover, local mineral resources are abundant, with a proven coal reserve of approximately 30 billion tons and a lignite coal field with the thickest coal seam and the largest reserve in China at present. In recent years, with rising coal production and accelerating

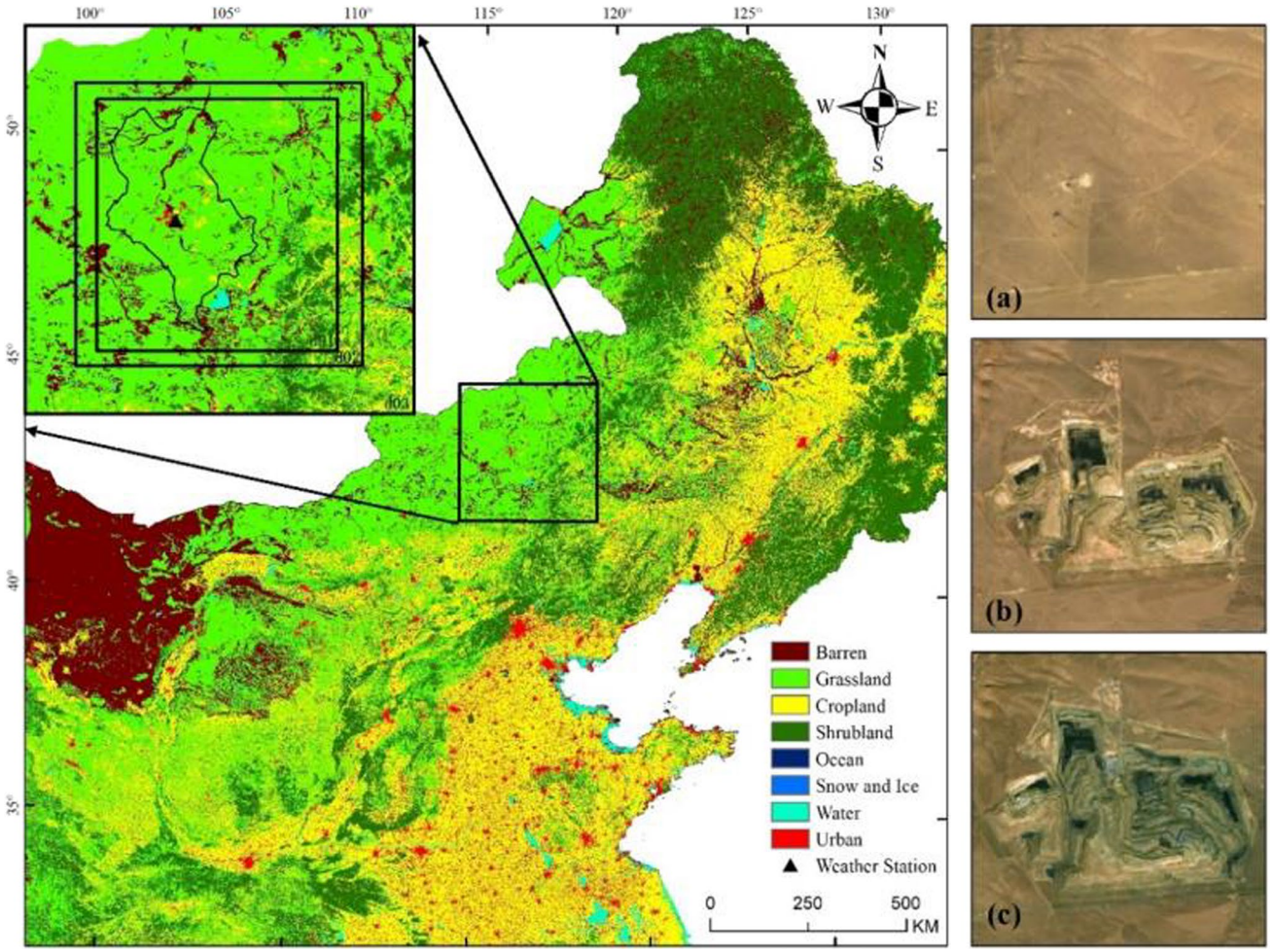

Fig. 1 The study area and three nested model domains used in the WRF simulations: (**a**) land status before mining, (**b**) land status during mining, and (**c**) land status after mining

urbanization, local grasslands have shown serious degradation, and the land is severely wind-eroded and sandy. At present, 45% of the total area of the Xilingol grassland is in a serious state of wind erosion and is becoming sandy, and 59.5% of the area is in a state of soil erosion. The serious degradation of land and grassland has led to the reduction in local species diversity, lower productivity, and ecological environmental degradation, which has seriously affected the production and economic development of local people.

Data

The initial boundary conditions and atmospheric forcing variables used for WRF simulations in this paper are Global Forecast System final analyses (FNL) provided by the National Centers for Environmental Prediction (NCEP) (http://dss.ucar.edu/datasets/ ds083.2/), which is global-scale grid point information generated by the Global Data Assimilation System (GDAS) with a horizontal resolution of 1°×1° and a time interval of 6 h. The parameters include surface pressure, sea surface pressure, geopotential height, temperature, sea surface temperature, soil conditions, ice cover, relative humidity, wind speed, vertical motion, vorticity, and ozone (Alexandru and Sushama 2015; Fei and Dudhia 2001; Wen et al. 2015).

To describe the subsurface changes in the study area in more detail, this paper uses the land classification product of the Chinese Academy of Sciences (CAS), which has a spatial resolution of 30 m. The CAS classification system is a remote sensing-based land use/land cover (LULC) classification system designated by the CAS for the completion of the first environmental database in China; it adopts an internationally common 2-tier structure based on the spectral and textural information of remote sensing data and divides the LULC into 25 secondary categories based on 6 primary categories according to land cover characteristics, coverage, and anthropogenic use. The CAS classification system includes surface cover types such as paddy fields, dry land,

forested land, and urban land (Huang and Gao 2017; Jandaghian and Berardi 2020; Pian et al. 2012; Xiao et al. 2021).

WRF configuration and parameterization

The model used in the simulation is the next-generation mesoscale WRF system (version 4.0.1) jointly developed by the NCEP and National Center for atmospheric research (NCAR). The horizontal grid spacings of the first nested area, the second nested area, and the third nested area are 9 km, 3 km, and 1 km, respectively, and the third nested area covers the whole study area. The projection is a Lambert cone projection, and the vertical direction is set to 32 layers. The initial field and boundary field of the simulation use FNL information, and the center of the simulation experiment is located at 44.2° N, 116° E. The first 15 days of the simulation are the spin-up time, and the experimental results only after 15 days are analyzed (Chen et al. 2017; Guo 2017; Vorotilova et al. 2020).

The physical process scenarios for this simulation are determined by comparative analysis of various combinations of model physical scenarios in the simulation area (Table 1). Among them, since the Noah land surface process model better considers the physical processes of soil moisture, soil temperature, vegetation canopy, and other factors and simulates the interaction processes of heat, radiation, and other fluxes between land and air (Cao et al. 2016; Fu et al. 2019; Li et al. 2011), the Noah land surface process model is used in this paper for land surface process simulation.

Design of the experiment

In this paper, the environments in April and July are selected for simulation, corresponding to the spring and summer seasons of the year, respectively (Fan et al. 2015; Gohain et al. 2020; Kowsalya et al. 2020; Li et al. 2016; Shen et al. 2020; Song et al. 2010). In the simulation process for each season, 2 different sets of urban subsurface simulations are conducted: the first set of experiments uses the 1980 LULC information, as shown in Fig. 2a, in which the urban subsurface type of Xilinhot during this period was mainly grass, and the area of urban and built-up land was small because it was before the urbanization process; the second set of experiments uses the 2018 LULC information (Fig. 2b), in which the urban area in this period significantly increased, reflecting the characteristics of postrapid urban development. All the WRF model parameters are set as the same in both experiments, except for the LULC information.

To use high spatial resolution land use data in the WRF model, the existing CAS land classification products need to be converted to International Geosphere–Biosphere Programme (IGBP) classification system products. The meaning of the secondary categories in the CAS land classification system is basically the same as that of the IGBP categories. Therefore, in this experiment, the secondary categories of the CAS classification system are converted to the corresponding IGBP categories by direct conversion. The specific conversion rules are shown in Table 2.

The specific technological flow of this paper is shown in Fig. 3.

Simulation evaluation

To verify the accuracy of the simulation results, the simulation results of each season are compared with the observations of meteorological stations in the study area (station number 54102) in this paper. The Pearson correlation coefficient (r), root mean square error (RMSE), and mean absolute error (MAE) are used to evaluate the differences between the simulated results and the real observations; the relative entropy (KL scatter) is used to evaluate the differences between the simulated results and the real observations in terms of data distribution. The specific expressions are as follows.

$$r = \frac{\sum_{i=1}^{n}\left(T_{wrf} - \overline{T_{wrf}}\right)\left(T_{station} - \overline{T_{station}}\right)}{\sqrt{\sum_{i=1}^{n}\left(T_{wrf} - \overline{T_{wrf}}\right)^2}\sqrt{\sum_{i=1}^{n}\left(T_{station} - \overline{T_{station}}\right)^2}} \quad (1)$$

$$RMSE = \sqrt{\frac{1}{n}\sum_{i=1}^{n}\left(T_{wrf} - T_{station}\right)^2} \quad (2)$$

Table 1 WRF model physical scheme

	d03	d02	d01
Horizontal grid point spacing	9 km	3 km	1 km
Grid points	108×102	162×150	228×204
Microphysical processes	WSM-3	WSM-3	WSM-3
Cumulus solutions	Kain-Fritsch	Turn off	Turn off
Boundary layer solutions	YSU	YSU	YSU
Longwave radiation program	Rrtmg	Rrtmg	Rrtmg
Shortwave radiation program	Dudhia	Dudhia	Dudhia
Near-surface layer solution	Monin-Obukhov	Monin-Obukhov	Monin-Obukhov
Land surface process model	Noah	Noah	Noah

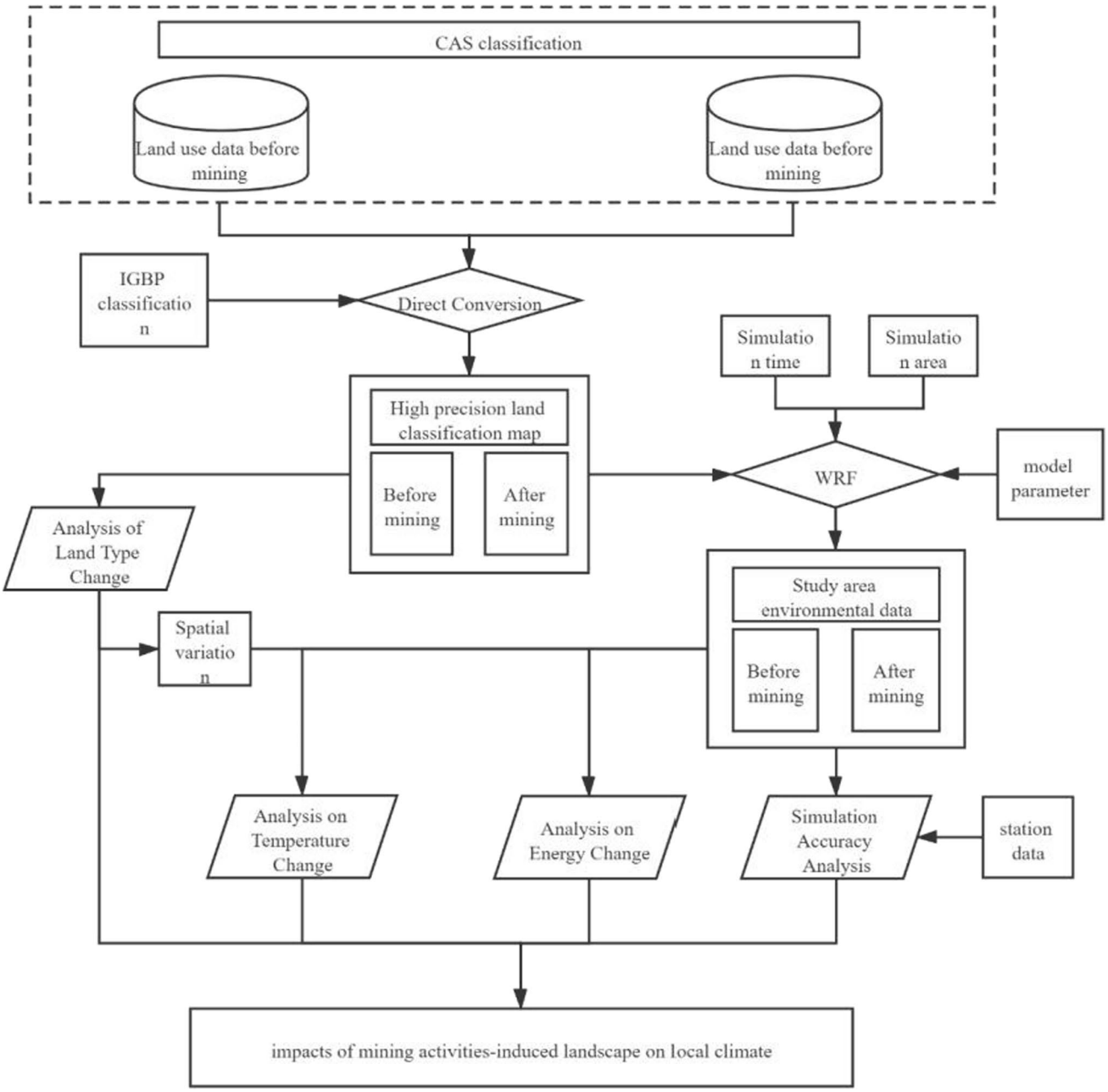

Fig. 2 Land use type change. (**a**) Land use type in 1980, (**b**) land use type in 2018, and (**c**) land use type change from 1980 to 2018

$$MAE = \frac{1}{n}\sum_{i=1}^{n} \mid T_{wrf} - T_{station} \mid \tag{3}$$

$$KL = \sum_{i=1}^{n} p\left(T_{wrf}\right) \ln\left(\frac{p\left(T_{wrf}\right)}{p\left(T_{station}\right)}\right) \tag{4}$$

where T_{wrf} is the WRF-simulated air temperature; $T_{station}$ is the observed temperature at the weather station; and n is the number of data points, i=1, 2, 3, ..., n.

Results

Land use change from 1980 to 2018

By analyzing the land type changes in the study area from 1980 to 2018, six main land cover types were found to exist in the area: sparse shrubs, typical grassland, cultivated land, urban and built-up land, bare land, and water bodies. Among them, typical grassland had the largest area, with an average of 88.710% and reached a peak of

Table 2 Correspondence between the CAS and IGBP classification systems

CAS secondary classification	IGBP classification
Water	Arable land
Dryland	
with forestland	Sparse shrubs
Shrubland	
Open woodland	
Other forestland	
Urban land	Urban and built-up land
Rural settlements	
Other construction land	
High-coverage grassland	Grassland
Medium-coverage grassland	
Low-coverage grassland	
Rivers and canals	Water bodies
Lakes	
Reservoir ponds	Water bodies
Beach	
Beach land	
Ocean	
Sand	Bare ground
Gobi Desert	
Saline land	
Marshland	
Bare land	
Bare rock	
Other	
Permanent glacial snow	Permanent ice and snow

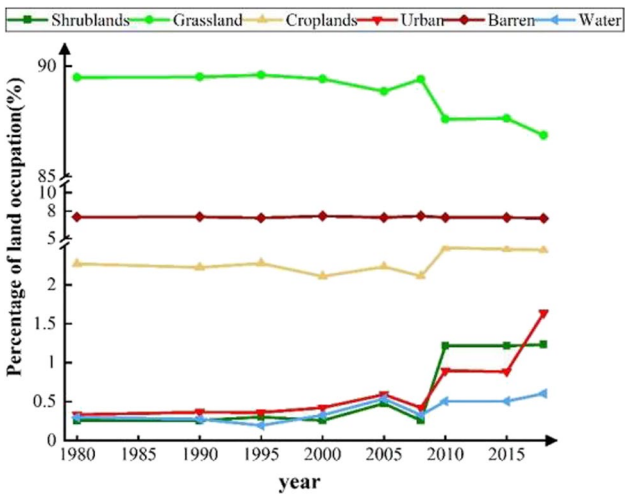

Fig. 3 Technological flow chart

89.605% in 1995; after 2000, the overall trend declined and reached a minimum of 86.874% in 2018. Among the remaining types, bare land had the largest area, with an average of 7.341% and a small variation over 38 years, with a variance of only 0.008, followed by cultivated land, with an average of 2.287%, showing a trend of decreasing and then increasing, with a minimum of 2.110% and a maximum of 2.472%. Urban and built-up land showed a more stable growth trend, from 0.332% in 1980 to 1.637% in 2018, an increase of nearly four times in 9 years, and the highest growth rate was nearly 1.126 times in 2010. Sparse shrubs and water bodies were the two categories with the lowest percentages, 0.608% and 0.396%, respectively.

The changes in land use types from 1980 to 2018 are shown in Fig. 4, which shows that 5.841% of the land underwent conversion. Among them, urban and built-up land and sparse shrubs changed the most, with area increases of 392.690% and 382.322%, respectively, but the original area of these two land use types was only 2.877%; thus, even though the change was large, the impact on the overall land use pattern was still limited. Grassland, which accounted for the largest area, changed from 89.509% in 1980 to 86.874% in 2018, a decrease of 2.944%, making it the land type with the largest net change. The smallest changes were in cropland and bare land, which changed by only 0.173% and −0.131%, respectively.

As shown by the land transfer matrix (Table 3), the conversion of grassland to built-up urban land and grassland to sparse shrubs were the most obvious, reaching 1.198% and 1.090%, respectively, which shows that during this 38-year period, the urbanization of Xilinhot city was obvious, while there was a certain tendency toward desertification.

Simulation validation

The simulated 2 m air temperature data for April and July were analyzed in comparison with the weather station observations (Fig. 5), and the accuracy evaluation results are shown in Table 4. The model performed well in spring and summer. The correlation coefficient (r) was 0.971 (p<0.01), and the RMSE was 2.040 K. The correlation coefficient (r) was 0.904 (p<0.01), and the RMSE was 2.469 K in summer, both of which are highly correlated with the observed data and have small relative errors. The correlation coefficient was 0.904 (p<01), and the RMSE was 2.469 K. The correlation coefficient was high, and the relative error was small. The distribution of the data shows that the simulation results were similar to the observations in all seasons, and the KL values were less than 0.001. Therefore, it can be concluded that the current physical parameters simulated the temperature variation within the study area well.

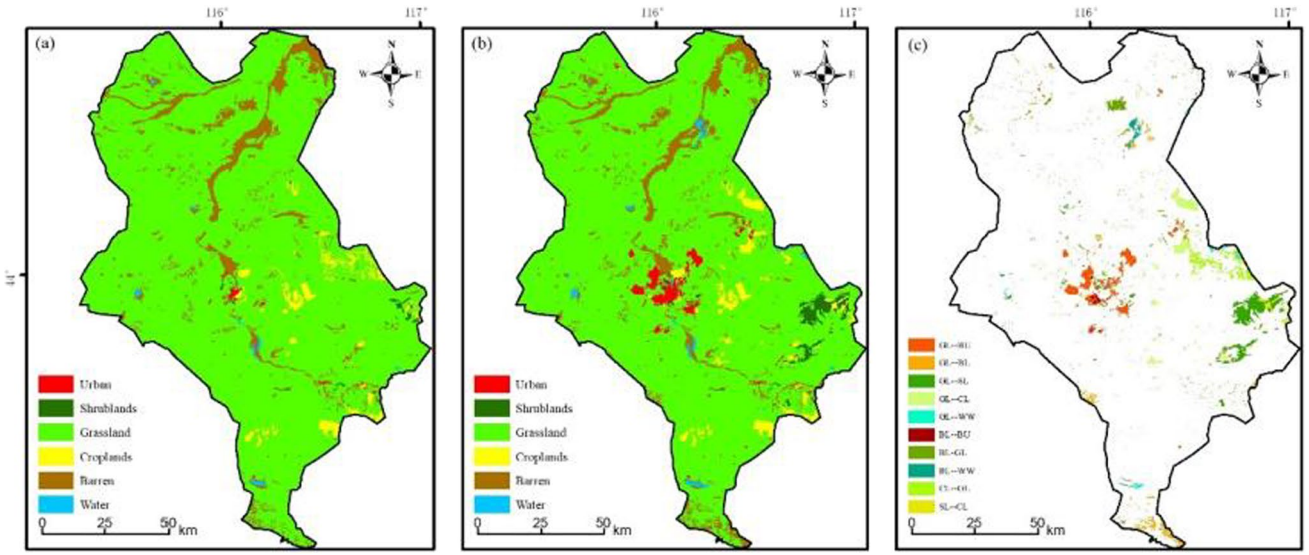

Fig. 4 Change in the land occupation rate

Table 3 Land transfer matrix for the Xilinhot region, 1980 to 2018

1980	2018						Total in 1980	Net change in 2018	Changes rate in 2018
	Grassland	Urban	Croplands	Barren	Water	Shrublands			
Grassland	85.524	1.198	0.753	0.810	0.134	1.090	89.509	−2.635	−2.944
Urban	0.014	0.313	0.001	0.001	0.000	0.002	0.333	1.307	392.690
Croplands	0.605	0.041	1.596	0.023	0.001	0.009	2.276	0.173	7.616
Barren	0.707	0.081	0.002	6.330	0.205	0.003	7.328	−0.131	−1.791
Water	0.005	0.000	0.000	0.031	0.262	0.000	0.297	0.305	102.523
Shrublands	0.018	0.006	0.098	0.001	0.000	0.134	0.257	0.981	382.322
Total (2018)	86.874	1.639	2.450	7.197	0.602	1.238	100.000		

Impacts of land use change on 2 m air temperature

Based on the experimental results, comparing the changes in spring and summer temperatures before and after the land use type change (Fig. 6), it can be concluded that for the average temperature, the overall average daily temperature in the spring of 2018 changed little compared to 1980, with a maximum warming of 2.820 K and a minimum cooling of 3.330 K. The overall average summer temperature decreased by 0.04 K, with a maximum warming of 9.6 K and a minimum cooling of 10.117K. For the maximum temperature, the average decrease in the study area was 0.049 K in spring and 0.072 K in summer. By comparing the average temperature, minimum temperature, and maximum temperature, it can be found that the impact of land use type change on summer temperature is greater than that on spring temperature. For the spatial distribution of temperature change, there was a clear difference between spring and summer distribution, with spring showing a decrease in temperature in most regions and an increase in temperature in the south. In summer, most areas showed significant warming, and cooling areas were scattered throughout the study area.

Separate temperature statistics for different land use type changes (Fig. 7) and for the average temperature (Fig. 7a) showed that the transition to water bodies caused the most drastic temperature changes, while the transition from bare land to water bodies lowered the regional temperature by an average of 5.278 K in summer, and the transition from grassland to water bodies lowered the regional temperature by an average of 1.349 K. In spring, these two transformations reduced the regional temperature by 0.668k and 1.725k, respectively. The next strongest change was the transition to urban and built-up land, where the transition from grassland to urban and built-up land increased the temperature by an average of 0.659 K in spring, the transition from bare land to urban and built-up land increased the temperature by an average of 0.901 K in summer, and the transition from grassland to urban and built-up land increased the temperature

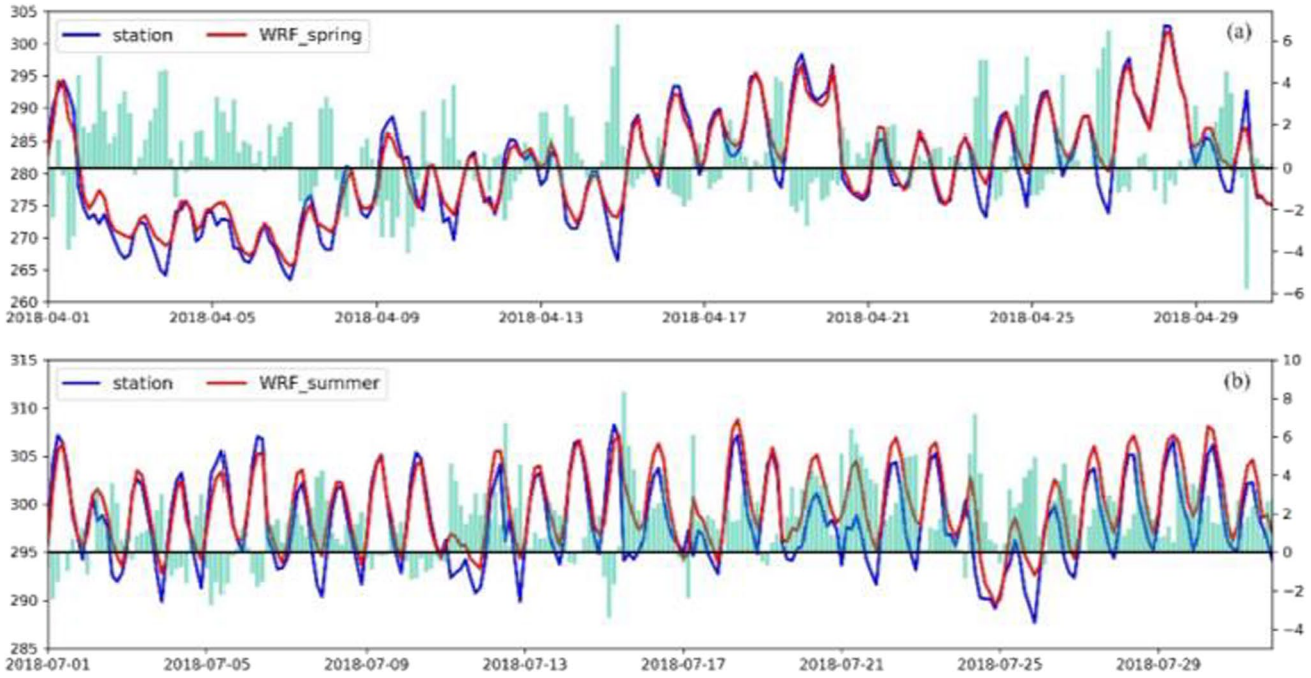

Fig. 5 Model accuracy validation. **a** Comparison between simulated data and stations in spring. **b** Comparison between simulated data and stations in summer

Table 4 Model accuracy validation

	r	*p*	RMSE	MAE	KL
Spring	0.9710	0.0000	2.0404	1.5583	0.0000
Summer	0.9042	0.0000	2.4685	1.9414	0.0000

by an average of 0.680 K in summer. Other land types had a smaller effect on temperature, but most of the changes had opposite effects on temperature in spring and summer, with the changes from grassland to cropland and from grassland to grassland causing an increase in temperature in spring and a decrease in temperature in summer; the three changes from grassland to grassland, from grassland to sparse shrubs and from sparse shrubs to cropland caused a decrease in temperature in both spring and summer. The three changes from grassland to bare ground, grassland to sparse shrubs, and sparse shrubs to cropland caused a decrease in temperature in spring and an increase in temperature in summer.

The minimum temperature statistics due to the conversion to different land use types (Fig. 7b) showed that the change to built-up urban areas caused a significant increase in the minimum temperature in the region in both spring and summer, with an average increase of 1.237 K in spring; the change from grassland to built-up urban land caused a minimum temperature increase of 1.164 K, and the change from bare land to built-up urban land caused a temperature increase of 1.311 K. The most dramatic change in minimum temperature occurred in the summer, when the change from bare land to water bodies resulted in a decrease of 3.234 K, far exceeding the temperature change caused by the other land use changes. The other transitions to water bodies did not have the same effect, with the grassland-to-water transition increasing the temperature by 0.064 K in summer; the transition to water bodies increased the temperature by an average of 0.229 K in spring; the grassland-to-water transition increased the temperature by 0.336 K; and the bare ground-to-water transition increased the temperature by 0.121 K. These changes indicate that water bodies have a certain warming effect at low temperatures.

For the change in maximum temperature, the statistical plot (Fig. 7c) shows that most of the conversion types had an insignificant effect on the maximum temperature, and only the two types of conversion to water bodies produced a very significant cooling effect. In spring, water bodies reduced the maximum temperature by an average of 2.990 K, with the conversion from bare land to water bodies causing a cooling of 3.997 K and the conversion from grassland to water bodies causing a cooling of 1.983 K. In summer, the water bodies decreased the maximum temperature by an average of 4.977 K, of which the conversion of bare land to water bodies and the conversion of grassland to water bodies cooled the temperature by 7.256 K and 2.698 K, respectively. In addition, built-up urban land did not affect the maximum temperature as much as it did the minimum temperature; the conversion of grassland to built-up urban land and the

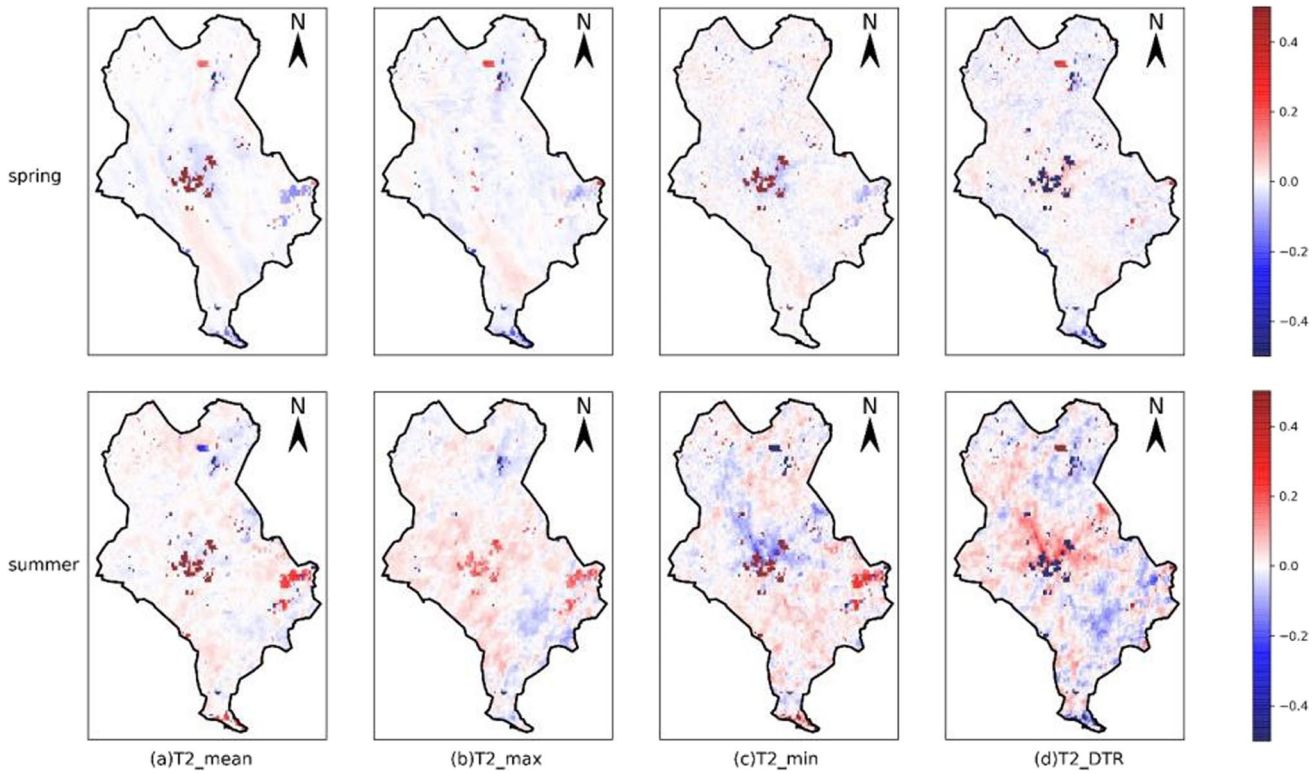

Fig. 6 Spatial pattern of temperature variation between spring and summer: (a) difference in the mean daily mean 2 m temperature, (b) difference in the maximum daily mean 2 m temperature, (c) difference in the minimum daily mean 2 m temperature, (d) difference in the diurnal temperature range (DTR) (K) of the daily mean 2 m temperature range

conversion of bare land to built-up urban land increased the maximum temperature by 0.002 K and 0.136 K in spring and 0.129 K and 0.186 K in summer, respectively, which are much less than their effects on the minimum temperature.

By using the daily maximum and minimum temperatures, the diurnal temperature difference was calculated (Fig. 6d), and observing its spatial distribution, the diurnal temperature difference significantly decreased in the built-up urban area, but the diurnal temperature difference increased in its periphery, and this phenomenon was especially obvious in summer. Statistical changes in daily temperature differences caused by the conversion of different land types (Fig. 7d) showed that in the whole study area, both the conversion to urban construction and water bodies caused significant decreases in diurnal temperature differences. In spring, the conversion from grassland to urban and built-up land caused a decrease of 1.162 K, the conversion from bare land to urban and built-up land caused a decrease of 1.175 K, the conversion from grassland to water bodies caused a decrease of 2.319 K, and the conversion from bare land to water bodies caused a decrease of 4.118 K. In summer, the conversion of grassland to built-up urban land and bare land to built-up urban land decreased the temperature by 1.241 K and 1.047 K, respectively, and the conversion of grassland to water bodies and bare land to water bodies decreased the temperature by 2.762 K and 4.022 K, respectively.

From the above analysis, it can be concluded that urban land significantly raised the average temperature, and water bodies lowered the average temperature. Both types of land significantly reduced the diurnal temperature difference, but the reasons for the formation of this phenomenon are different. Urban and built-up land raised both the minimum and maximum temperatures, but the increase in the minimum temperature was much greater than the increase in the maximum temperature, thus producing a reduction in the diurnal temperature difference. Water bodies, on the other hand, significantly lowered the maximum temperature and raised the minimum temperature to achieve the effect of a lower diurnal temperature difference. For other types of transitions, the resulting effects were not significant.

Impacts of land use change on the surface energy budget

In order to analyze the impact of land use types on temperature comprehensively, it is necessary to analyze the effect of different land use types on surface energy balance. The following figure illustrates the effect of land use type change on

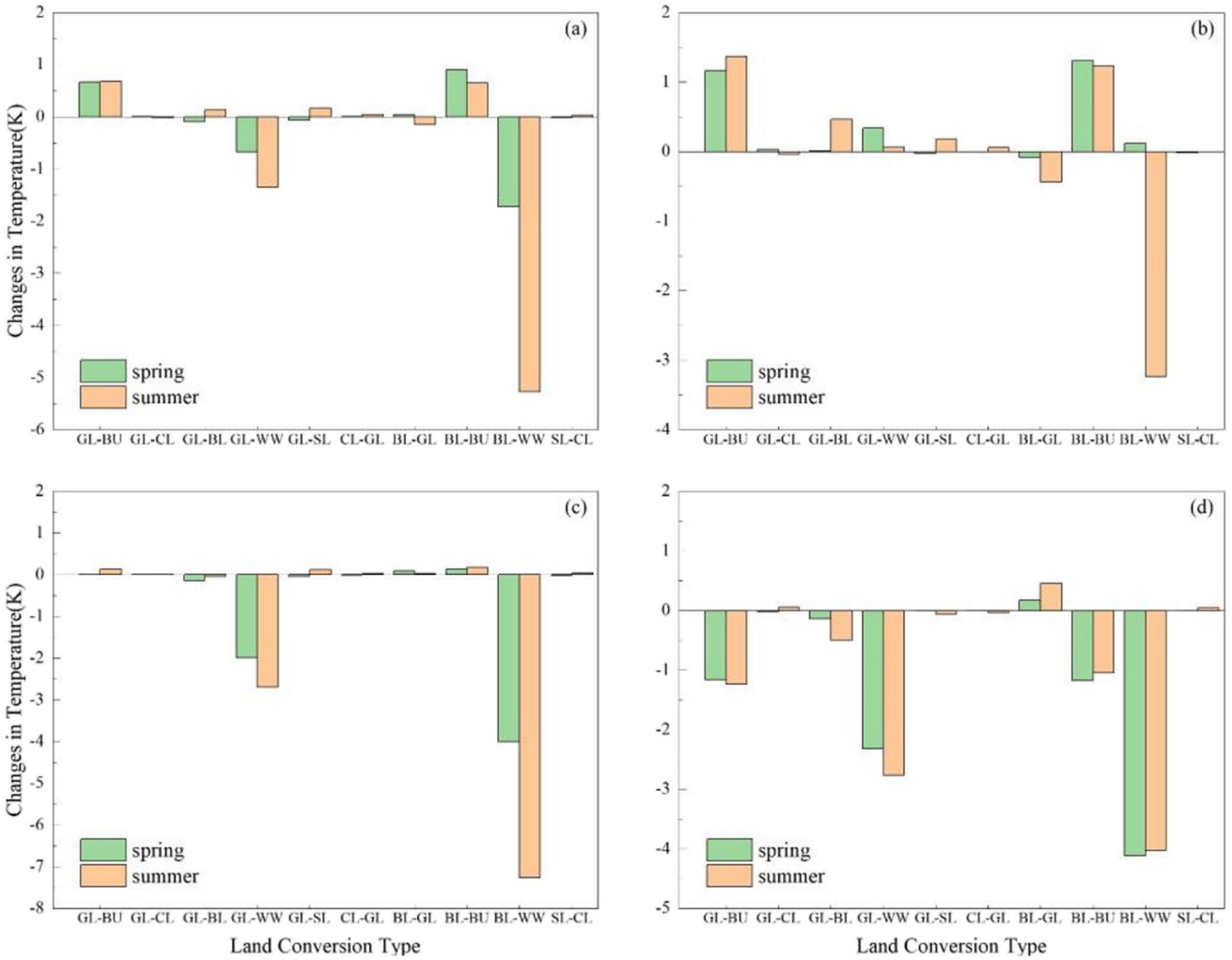

Fig. 7 Effect of different land use conversion types on temperature, (**a**) average temperature, (**b**) minimum temperature, (**c**) maximum temperature, and (**d**) diurnal temperature. GL, BU, CL, BL, SL, and WW represent grassland, built-up urban land, cropland, bare land, sparse shrubs, and water bodies, respectively

the latent heat flux (LH), sensible heat flux (SH), and surface heat flux (GRD) during daytime and nighttime. The effect of land use change in the daytime is more complex than that in the nighttime. In general, the daytime LH of the whole study area before and after the change was 41.907 W/m^2 and 41.423 W/m^2, respectively, with an average decrease of 0.487 W/m^2. The conversion to built-up urban land caused a significant decrease in LH values, the most obvious ones being the conversion from grassland to built-up urban land and the conversion from bare land to built-up urban land, which decreased by 13.888 W/m^2 and 21.983 W/m^2, respectively. The conversion to urban built-up land and the conversion of bare land to urban built-up land were the most obvious, decreasing by 13.888 W/m^2 and 21.983 W/m^2, respectively, while the nighttime LH was 2.617 W/m^2 and 2.660 W/m^2, increasing by 0.043 W/m^2 on average, and it did not produce significant changes between the conversions of each category.

In contrast to the LH, a different change in the SH was observed. The SH was 181.991 W/m^2 and 181.378 W/m^2 during the day in both experiments, with an average decrease of 0.616 W/m^2 in 2018 compared to 1980. Unlike the effect on the LH, the conversion to built-up urban land caused an increase in the SH, most notably the conversion of bare land to built-up urban land, which increased the SH by nearly 26.252 W/m^2. During the nighttime hours, the SH was −17.709 W/m^2 and −17.366 W/m^2 for the two experiments, with an average increase of 0.342 W/m^2. In contrast to the LH, each land type conversion did not cause a large SH change.

The GRD, as one of the key terms of energy expenditure, is influenced by net radiation and directly related to the thermodynamic properties of the subsurface. When the GRD value is less than 0, it means that heat enters the soil, and conversely, when the GRD value is greater than 0, it

means that heat is released from the soil to the surface (Elizabeth et al. 2018; Nambiar et al. 2020). During the daytime, the GRD of the two experiments were −118.07 W/m^2 and −118.412 W/m^2, with an overall average decrease of 0.753 W/m^2. The conversion of grassland, cropland, and bare land to built-up urban land resulted in larger changes of −33.781 W/m^2, −11.787 W/m^2, and −56.145 W/m^2, respectively, while built-up urban land without conversion also produced a change of −15.822 W/m^2, indicating that urbanization also had a large impact on the original urban area. At night, however, the conversion to built-up urban land still caused a significant change in GRD values compared to the other conversions, but not as dramatic as during the day, most notably with the conversion of bare land to built-up urban land, which caused a change of 14.899 W/m^2.

From the above analysis, it is revealed that for the whole region, the energy changes caused by built-up urban land are the most significant, which also led to more significant temperature changes in these regions. Built-up urban land reduced the LH value and allowed more energy to be used

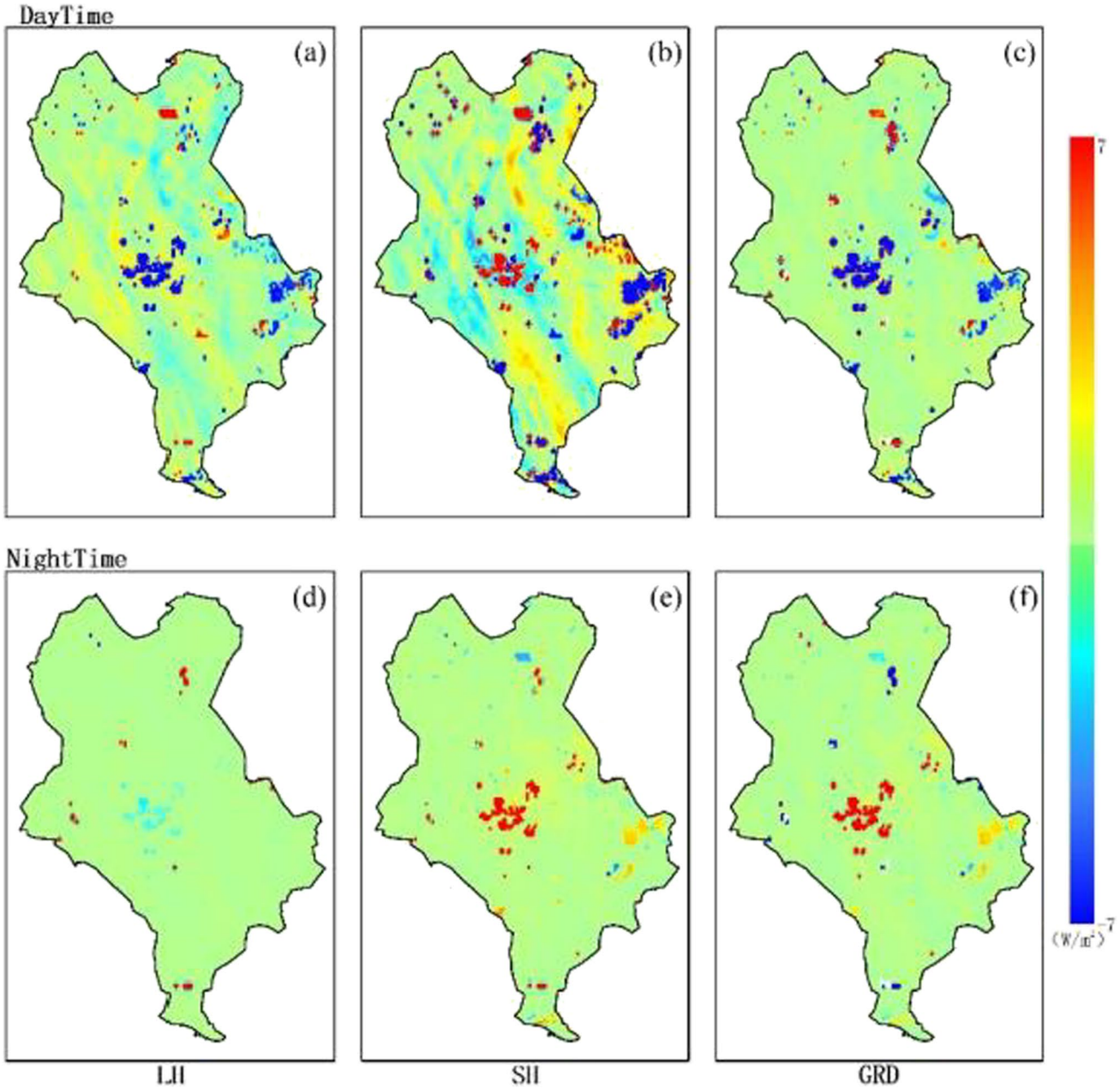

Fig. 8 Diurnal energy variation. (**a**) LH of daytime, (**b**) SH of daytime, (**c**) GRD of daytime, (**d**) LH of nighttime, (**e**) SH of nighttime, and (**f**) GRD of nighttime

Table 5 Daytime energy variation

1980												
2018	Grassland			Urban			Cropland			Bare land		
	LH	SH	GRD	LH	SH	GRD	LH	SH	GRD	LH	SH	GRD
Grassland	−0.239	−0.298	−0.327	−0.713	1.654	0.051	−1.813	3.966	1.106	2.553	15.033	1.851
Urban	−13.888	6.692	−33.781	−6.112	5.447	−15.822	−5.945	−3.731	−11.787	−21.983	26.252	−56.145
Cropland	1.137	−5.283	−2.602	0.000	0.000	0.000	−0.645	1.438	−1.908	0.560	−0.877	−0.201
Bare land	−2.456	−18.302	−0.020	0.000	0.000	0.000	−0.979	1.261	−0.330	−0.289	−0.174	0.215

to raise the SH value, which also led to significantly higher urban temperatures than other land types. The impervious surfaces used for urbanization were more likely to absorb heat during the day than ordinary land, which allowed more energy to enter the soil during the day and raise the surface temperature and more energy to be released as heat during the night, which is why urbanization reduced the temperature difference between day and night. Additionally, because of the impermeable surface, the energy changed more dramatically during the day than during the night (Fig. 8) (Tables 5 and 6).

Discussion

In this study, we used high-resolution land use data to simulate and assess the climate of Xilinhot city. Due to urbanization and coal mining, the built-up urban land in Xilinhot city changed significantly during 1980–2018. The changes in ground conditions have a significant impact on the local climate. Vegetation changes directly affect the regional climate through energy exchange between the ground and air; however, this feedback can be complex. Compared with the land use data which is low and medium resolution used in the previous study (Bhati and Mohan 2018; Ma et al. 2009). The 30-m land use data in this study can improve the simulation accuracy of WRF model in the impact of land use change on the spring and summer climate of Xilinhot. The high correlation coefficient and low model bias between the model simulations and observations showed the good performance of the model. The results showed that land use type changes have a greater impact on summer temperatures in Xilinhot than in spring, urban land can significantly increase the average temperature, and water bodies can decrease the average temperature. Both types of land use significantly reduce the diurnal temperature difference, but the reasons for this phenomenon are different. Urban land use increases both the minimum and maximum temperatures, but it increases the minimum temperature much more than the maximum temperature, thus producing a reduction in the diurnal temperature difference. Water bodies, on the other hand, significantly decrease the maximum temperature and increase the minimum temperature to achieve the effect of a lower diurnal temperature difference. In addition, the study analyzed the impact of land use change on earth atmosphere energy exchange, explaining the reasons for the impact of land use on temperature in the perspective of energy change. For the diurnal energy change, the energy change caused by urban construction sites is the most obvious. The increase in urban construction sites causes a surge in the area of impermeable surfaces, which allows more energy to enter the soil during the day while reducing the latent heat flux, thus allowing more energy to flow via the sensible heat flux, which leads to high temperatures in urban areas. At night, the energy in the soil starts to be released as heat, which leads to higher nighttime temperatures, which in turn leads to lower diurnal temperature differences in urban areas.

Due to the limitation of data, we only use the land use data for 1980 and 2018 in the numerical simulations, which do not fully reflect the land use change during the whole study period. Moreover, the experiment only changes the land use, did not change the vegetation, such as NDVI, and

Table 6 Nocturnal energy changes

1980												
2018	Grassland			Urban			Cropland			Bare land		
	LH	SH	GRD	LH	SH	GRD	LH	SH	GRD	LH	SH	GRD
Grassland	0.011	0.198	0.082	−0.036	0.007	0.060	0.000	−0.323	−0.419	0.443	−0.285	−0.859
Urban	−0.746	5.819	9.256	−0.415	2.811	4.294	−0.308	2.502	3.259	−1.400	8.651	14.899
Cropland	−0.090	0.972	0.947	0.000	0.000	0.000	−0.057	0.400	0.541	−0.012	0.305	0.044
Bare land	0.450	1.268	−0.373	0.000	0.000	0.000	−0.082	0.446	0.206	0.127	0.298	−0.194

this is something that can be improved. In addition, this study is mainly based on numerical experiments, and the uncertainty of simulation results cannot be avoided.

Conclusions

In this study, the WRF model was used to quantitatively assess the climate transformations caused by land use changes in Xilinhot city. From 1980 to 2018, the main vegetation types in Xilinhot city did not change substantially, but the physical properties of the land surface were changed due to the increasing built-up urban area due to coal mining and urbanization. However, the average local temperature did not increased, which is mainly because the main land types in the area did not change substantially, and the significant temperature changes were mainly concentrated in the areas converted to urban and built-up land and water bodies. The urban and built-up land warmed, while the water bodies had a significant cooling effect, which was particularly pronounced in summer. At the same time, both types of land conversion caused a reduction in diurnal temperature differences. This temperature shift was directly related to the change in energy distribution between the land and air, with urban and built-up land enabling more energy to be used to raise SH values, resulting in significantly higher urban temperatures than in other land types. The results of the study showed that although the average temperature change from 1980 to 2018 was not significant, mainly due to the vast grassland area in the region, local changes in temperature and energy aggregation were obvious, and uncontrolled coal mining and urban expansion will most likely cause abrupt changes in the climate of the region in some places, which will affect the whole region.

Author contribution HongRu Bi: software, validation, writing—original draft preparation, Wei Chen: conceptualization, methodology, writing—reviewing and editing, supervision. Jun Li: data curation. Junting Guo: software. Changchao She: investigation.

Funding This research is funded by the National Natural Science Foundation of China (Grant Nos. 41701391, 41601348, and 61841101). Fundamental Research Funds for the Central Universities (Grant number 2022JCCXDC04, 2022YJSDC14), and Yueqi Young Scholar Project of China University of Mining and Technology-Beijing.

Data availability The datasets used and/or analyzed during the current study are available from the corresponding author on reasonable request.

Declarations

Ethics approval and consent to participate Not applicable.

Consent for publication Not applicable.

Competing interests The authors declare no competing interests.

References

Alam MS, Barbour SL, Huang M, Li Y (2020) Using statistical and dynamical downscaling to assess climate change impacts on mine reclamation cover water balances. Mine Water Environ 39:699–715

Alexandru A, Sushama L (2015) Impact of land-use and land-cover changes on CRCM5 climate projections over North America for the twenty-first century. Climate Dynam 47:1197–1209

Bhati S, Mohan M (2018) WRF-urban canopy model evaluation for the assessment of heat island and thermal comfort over an urban airshed in India under varying land use/land cover conditions. Geosci Lett 5:1–19

Bollasina M, Nigam S (2011) Modeling of regional hydroclimate change over the Indian subcontinent: impact of the expanding Thar Desert. J Climate 24:3089–3106

Cao Q, Yu DY, Georgescu M, Wu JG (2016) Impacts of urbanization on summer climate in China: an assessment with coupled land-atmospheric modeling. J Geophys Res Atmos 121:10505–10521

Chen L, Ma Z, Zhao T (2017) Modeling and analysis of the potential impacts on regional climate due to vegetation degradation over arid and semi-arid regions of China. Climatic Change 144:461–473

Chen LY, Liu CX (2006): Study on land use/cover change in Xilinhot city. Bull Soil Water Conserv 26, 60-64+111

Elizabeth B, Ahmed T, Andrew O, Lucie L, Kimberly N, Scott O, Colin Z, Gordon B (2018) The role of surface roughness, albedo, and Bowen ratio on ecosystem energy balance in the Eastern United States. Agri Forest Meteorol 249:367–376

Fan X, Ma Z, Yang Q, Han Y, Mahmood R (2015) Land use/land cover changes and regional climate over the Loess Plateau during 2001–2009. Part II: interrelationship from observations. Climatic Change 129:441–455

Fei C, Dudhia J (2001) Coupling an advanced land surface-hydrology model with the Penn State-NCAR MM5 modeling system. Part I: model implementation and sensitivity. Monthly Weather Rev 129:569–585

Fu P, Xie Y, Weng Q, Myint S, Meacham-Hensold K, Bernacchi C (2019) A physical model-based method for retrieving urban land surface temperatures under cloudy conditions. Remote Sens Environ 230:111191

Gohain KJ, Mohammad P, Goswami A (2020) Assessing the impact of land use land cover changes on land surface temperature over Pune city, India. Quaternary Intl 575-576:259–269

Guo F (2017) Assessment method of urban heat island high resolution based on WRF. J Civil Environ Eng(in Chinese) 039:13–19

Huang D, Gao S (2017) Impact of different reanalysis data on WRF dynamical downscaling over China. Atmos Res 200:25–35

Inta T, Somprasong K, Huttagosol P (2020) Study of climate effect on the atmospheric conversion in coal mine: a case study of lignite coal mine in Thailand. IOP Conf Ser Earth Environ Sci 581:012028

Jandaghian Z, Berardi U (2020) Comparing urban canopy models for microclimate simulations in weather research and forecasting models. Sustain Cities Soc 55:102025

Kowsalya T, Ullo SL, Zarro C, Hemalatha KL, Parameshachari BD (2020) Land use and land cover classification using a human group based particle swarm optimization algorithm with a LSTM classifier on hybrid-pre-processing remote sensing images. Remote Sens 12:4135

Larondelle N, Haase D (2012) Valuing post-mining landscapes using an ecosystem services approach—an example from Germany. Ecol Indicators 18:567–574

Li J, Zhao Y, Liu H, Su Z (2016) Sandy desertification cycles in the southwestern Mu Us Desert in China over the past 80years recorded based on nebkha sediments. Aeolian Res 20:100–107

Li N, Yan CZ, Xie JL (2015) Remote sensing monitoring recent rapid increase of coal mining activity of an important energy base in northern China, a case study of Mu Us Sandy Land. Resour Conserv Recyc 94:129–135

Li X, Yang XQ, Tang JP (2011) Multiple urban heat islands and surface energy balance during summer in Yangtze River Delta city cluster region simulated with WRF/NCAR. J Meteorol Sci 31:441–450

Liu JY, Shao QQ, Yan XD (2011) An overview of the progress and research framework on the effects of land use change upon global climate. Adv Earth Sci(in Chinese) 26:1015–1022

Ma HY, Guo P, Jie AS (2009) Simulation of "2007.7" Heavy rainfall case in the Changjiang-Huaihe valley using the WRF model with different land surface schemes. Chinese J Atmos Sci 33:557–567

Nambiar MK, Robe FR, Seguin AM, Endsin M, Aliabadi AA (2020) Diurnal and seasonal variation of area-fugitive methane advective flux from an open-pit mining facility in Northern Canada using WRF. Atmosphere 11:1227

Pang L, Su X (2010) Using thematic mapping images for Xilinhaote cityscape spatial layout analysis. Planners 26:45–48

Pang L, Shun NA (2011) Temporal-spatial characteristics of landscape pattern in Xilinhot. Ecol Econ 235:151-154 +158

Pian XD, Li X, Ran YH, Liu C (2012) Influence of underlying surface on regional climate accuracy of WRF model in Heihe River Basin. Plateau Meteorol(in Chinese) 31:657–667

Qian D, Yan C, Xiu L, Feng K (2018) The impact of mining changes on surrounding lands and ecosystem service value in the Southern Slope of Qilian Mountains. Ecol Complexity 36:138–148

Schueler V, Kuemmerle T, Schroeder H (2011) Impacts of surface gold mining on land use systems in Western Ghana. Ambio 40:528–539

Shen Y, Shen HF, Cheng Q, Zhang L (2020) Generating comparable and fine-scale time series of summer land surface temperature for thermal environment monitoring. IEEE J Select Top Appl Earth Observ Remote Sens 14:2136–2147

Song K, Zhao J, Wei O, Zhao X, Hao F (2010) LUCC and landscape pattern variation of wetlands in warm-rainy Southern China over two decades. Procedia Environ Sci 2:1296–1306

Vorotilova PG, Konstantinov PI, Varentsov MI, Timazhev AV, Baklanov AA (2020) Study of surface-based temperature inversions in the city of Nadym (Western Siberia) with direct measurements and numerical simulation. IOP Conference Ser Earth Environ Sci 611:012021

Wang MN, Han Z, Zhang QY (2016) Effects of land use change on surface temperature in semi-arid areas of northern China in the early 21st century. Climate Environ Stud(in Chinese) 21:65–77

Wang X, Guo W, Bo Q, Ye L, Ding A (2017) Quantifying the contribution of land use change to surface temperature in the lower reaches of the Yangtze River. Atmos Chem Phys 17:4989–4996

Wang YL, Feng JM, Hao G (2014) Numerical simulation of the impact of land cover change on regional climate in China. Theor Appl Climatol 115:141–152

Wei JS, He X, Hu CY, Wang J (2006): Effect of coal mining subsidence on sandy soil moisture characteristics in arid and semi-arid areas. Resources and environment in Arid Areas(in Chinese), 84-88

Wei TT, Hu ZQ, Cao YB, Li XY, Chen C (2015) Effects of coal mining on soil physical properties and crust in aeolian sand area. Water Soil Conserv Bull(in Chinese) 35:106–110

Wen XH, Dong WJ, Liao XH (2015) Simulation of radiation budget and energy balance in summer in Northeast Semi-arid Region by WRF model. J Solar Energy(in Chinese) 36:2196–2203

Wu Q, Pang J, Qi S, Li Y, Han C, Liu T, Huang L (2009) Impacts of coal mining subsidence on the surface landscape in Longkou city, Shandong Province of China. Environ Earth Sci 59:783–791

Wu QY, Feng ZW, Hu ZQ, Chen C, Fu YK, Yang FQ, Gao LL (2020) Influence of dynamic change of surface cracks on soil water content in ecologically fragile mining areas. Coal Sci Technol(in Chinese) 48:153–160

Xiang H, Wang Z, Mao D, Zhang J, Zhao D, Zeng Y, Wu B (2021) Surface mining caused multiple ecosystem service losses in China. J Environ Manage 290:112618

Xiao YX, Wu Z, Fang DX, He J, Tang JP (2021) Effects of urbanization on summer temperature change in the Sichuan basin from observation and simulation. Geophys(in Chinese) 64:100–113

Xiu L, Yan C, Li X, Qian D, Feng K (2018) Monitoring the response of vegetation dynamics to ecological engineering in the Mu Us Sandy Land of China from 1982 to 2014. Environ Monit Assess 190:543.1-543.18

Zhang YX, Bi YL, Chen SL, Wang J, Han B, Feng YB (2015) Influence of fracture development on soil moisture after coal mining in semi-arid Aeolian Sandy Area. Environ Sci Technol(in Chinese) 38:11–14

Zheng Y, Dong L, Xia Q, Liang C, Shao Y (2020) Effects of revegetation on climate in the Mu Us Sandy Land of China. Sci Total Environ 739:139958